Apparent horizons for boosted or spinning black holes

Gregory B. Cook and James W. York, Jr.
Institute of Field Physics, Department of Physics and Astronomy, University of North Carolina, Chapel Hill, North Carolina 27599-3255
(Received 28 August 1989)

As part of an ongoing study of initial data for black-hole collisions, we examine the apparent horizons in initial-data sets for a single black hole with either translational or rotational velocity constructed using a systematic and easily generalized formalism. The apparent-horizon equation is formulated as a boundary-value problem that, with small changes, will be applicable to nonaxisymmetric problems. We find all apparent horizons in our numerically generated sets of initial data. A previously known exact result for spinning holes is reproduced numerically. We find new results, both exact and numerical, for the apparent horizons of black holes with linear momentum. In some of these cases an interesting structure emerges in which the apparent horizons and minimal surface intersect one another.

I. INTRODUCTION

One of the prime goals of numerical relativity is to simulate the fully three-dimensional spiraling collision of two black holes. There are many separate facets to the task of setting up, evolving, and interpreting the results of such a simulation. In Refs. 1–5, an analytic framework has been given upon which such simulations can be built by prescribing a method for determining the initial data for black holes with given linear and angular momentum. The method employs conformal transformations and a method of imaging applicable to tensors. We shall call it the conformal imaging method. Many authors have studied single-hole, axisymmetric initial-data sets using numerical methods based on this framework.[6–8] These authors have examined the total energy of the solutions and the consequences for the positive-energy theorem, the possible existence of naked singularities, and have estimated upper bounds on the energy associated with these holes in the form of gravitational radiation.

A very important feature of the initial-data sets built with the conformal imaging technique which has not been studied sufficiently is the existence and position of apparent horizons. Hawking and Ellis[9] show that an event horizon, which cannot be located without knowledge of the time development of the data, necessarily exists outside or coincident with an apparent horizon (subject to certain technical assumptions). The apparent horizon, on the other hand, is determined by the initial data. This allows the mass of the apparent horizon (essentially the square-root of its area) to be found and used as a lower limit on the irreducible mass of the event horizon. As a result, an upper limit on the amount of gravitational-wave energy in the system can be found.

The position of the apparent horizons for two black holes on a time-symmetric slice, in which the holes are momentarily at rest, has been studied by various authors.[10–12] Given that the slice is time symmetric, this amounts to finding minimal surfaces. These authors have relied on "shooting" methods for solving the minimal-surface equation. This is an appropriate method for situations where the surface is axisymmetric. However, this method cannot be applied to a general three-dimensional problem. Oohara, Nakamura, and Kojima[13,14] have outlined and tested a method for determining apparent horizons, based on an expansion in spherical harmonics, which is appropriate for general three-dimensional problems. An alternative approach for solving the fully three-dimensional apparent-horizon equation is to set it up as a boundary-value problem.

There are two principal aims of this work. First, we will find and characterize in physical terms the apparent horizons associated with a number of cases of initially purely spinning or initially purely translating single black holes. Second, we will locate the apparent horizons by solving numerically a nonlinear boundary-value problem whose input includes the numerically generated solution of another nonlinear boundary-value problem (the Hamiltonian constraint). We have chosen this method for our axisymmetric configuration because, with minor changes, it will be applicable to general three-dimensional problems such as the data for the rotating coalescence of two black holes. In the case of spinning holes, we are able to reproduce numerically with high accuracy a known result. We find new results, both exact and numerical, for the apparent horizons of black holes with linear momentum. In some of these cases a novel structure emerges in which apparent horizons intersect the minimal surface joining the two sheets of the complete three-manifold that models the black hole. This causes the black hole to appear partly as a black hole and partly as a "white hole" in a sense to be described.

We begin with a brief review of the conformal imaging formalism for single black holes with linear or angular momentum. Next, we describe our numerical solution of the Hamiltonian constraint. A key feature of the conformal imaging formalism is the isometry imposed between the two asymptotically flat sheets that form the initial hypersurface and model the initial geometry of the black hole. We derive explicitly the consequences of this symmetry and employ it in solving for the apparent horizons. In the final sections, we find and discuss the solutions.

II. THE CONFORMAL IMAGING FORMALISM

In Refs. 1–5 there is given a formalism for solving the vacuum constraint equations when the initial hypersurface is a maximal slice of the space-time and when the slice is conformally and asymptotically flat. The method takes the initial slice to consist of two isometric asymptotically flat spacelike hypersurfaces connected by N throats, with each throat representing a black hole. In this work we will only deal with the special case of one hole.

As in Ref. 3, the vacuum Einstein constraint equations are written

$$\bar{\nabla}^j(\bar{K}_{ij}-\bar{g}_{ij}\bar{K})=0 , \tag{1}$$

$$\bar{R}-\bar{g}^{im}\bar{g}^{jn}\bar{K}_{ij}\bar{K}_{mn}+\bar{K}^2=0 . \tag{2}$$

$\bar{K}_{ij}$ is the extrinsic curvature, $\bar{K}=\bar{g}^{ij}\bar{K}_{ij}$, and $\bar{R}$ is the scalar curvature of the hypersurface with three-metric $\bar{g}_{ij}$. The hypersurface is assumed to be conformally flat so that $\bar{g}_{ij}=\psi^4 g_{ij}$ (g_{ij} is a general flat metric) and maximally embedded so that $\bar{K}=0$. In our notation, objects with overbars are defined on the physical space and corresponding objects without an overbar are defined on the conformally related "background" space. Taking $\bar{K}_{ij}=\psi^{-2}K_{ij}$, the constraint equations become

$$\nabla^j K_{ij}=0 \tag{3}$$

and

$$\nabla^2\psi=-\tfrac{1}{8}K_{ij}K^{ij}\psi^{-7} . \tag{4}$$

The two asymptotically flat hypersurfaces which form the initial slice are usually referred to as the "top" and "bottom" sheets of the slice. The two sheets are joined at the "throat" which is a fixed-point set of the isometry relating the two sheets. The isometry is defined by an inversion map denoted by $x'^i=J^i(x^1,x^2,x^3)$ with Jacobian $J^i_j=\partial J^i/\partial x^j$. Demanding that the two physical sheets be isometric forces the following conditions on the physical metric and extrinsic curvature:

$$\bar{g}_{ij}(x)=J^k_i J^l_j \bar{g}_{kl}[J(x)] , \tag{5}$$

$$\bar{K}_{ij}(x)=\pm J^k_i J^l_j \bar{K}_{kl}[J(x)] . \tag{6}$$

Bowen and York[3] follow Misner[15] and take the inversion map to be defined by inversion through a sphere. Using spherical coordinates for the flat background metric g_{ij}, the mapping becomes

$$r'=\frac{a^2}{r}, \quad \theta'=\theta, \quad \phi'=\phi , \tag{7}$$

where $r=a$ labels the throat which is the surface of inversion.

Bowen and York[3] found a set of solutions of (3) which obey the isometry conditions (6) and which carry, respectively, linear and angular momentum. These solutions are

$$K^{\pm}_{ij}=\frac{3}{2r^2}[P_i n_j+P_j n_i-(g_{ij}-n_i n_j)P^k n_k] \mp\frac{3a^2}{2r^4}[P_i n_j+P_j n_i+(g_{ij}-5n_i n_j)P^k n_k] , \tag{8}$$

$$K_{ij}=\frac{3}{r^2}(\epsilon_{kil}J^l n^k n_j+\epsilon_{kjl}J^l n^k n_i) , \tag{9}$$

where P^i and J^i are constant vectors and n^i is an outward-pointing unit normal of a sphere. K^+_{ij} satisfies condition (6) with the plus sign. K^-_{ij} and K_{ij} satisfy condition (6) with the minus sign. That P^i and J^i represent, respectively, the total *physical* linear and angular momenta can be seen by substituting (8) and (9) into the surface-integral formulas[1] and recalling that $\psi=1+O(r^{-1})$ for large r, so that either K_{ij} or $\bar{K}_{ij}$ can be used in these integrals.

Using (7), Bowen and York[3] have shown that the surface of inversion is extremal with respect to area and proved in a wide set of cases that it must be minimal. Because we know of no counterexample, we assume that the throat is a minimal surface. That this surface is an extremal surface implies a differential condition on the conformal factor ψ which must be satisfied at the surface of inversion. This condition,

$$\left[\frac{\partial\psi}{\partial r}+\frac{1}{2a}\psi\right]_{r=a}=0 , \tag{10}$$

can be used as an inner boundary condition for ψ. Equation (10) in conjunction with an outer boundary condition for ψ makes (4), the Hamiltonian constraint, a well-posed elliptic boundary-value problem for ψ. The uniqueness of solutions of the Hamiltonian constraint has been shown using the boundary condition (10) above by means of a local uniqueness proof.[16] [It should be noted that (10) has the *wrong* relative sign for a standard uniqueness proof to suffice.]

III. NUMERICAL SOLUTION OF THE HAMILTONIAN CONSTRAINT

The Hamiltonian constraint is a nonlinear elliptic equation and must in general be solved numerically. Numerical solutions of the Hamiltonian constraint following the conformal imaging formulation have been carried out by several authors[6–8] and we will not dwell long on it here.

It is efficient in numerical work to use spherical coordinates with the additional coordinate transformation

$$r=ae^x . \tag{11}$$

In these coordinates, the domain of the top sheet is $0<x\le\infty$ and the domain of the bottom sheet is $-\infty\le x<0$. The minimal surface is at $x=0$. Using a Robin outer boundary condition as described in York and Piran,[6] the Hamiltonian constraint becomes

$$\left[e^{-x}\frac{\partial}{\partial x}\left[e^x\frac{\partial\psi}{\partial x}\right]+\frac{1}{\sin\theta}\frac{\partial}{\partial\theta}\left[\sin\theta\frac{\partial\psi}{\partial\theta}\right]\right] +\frac{a^2e^{2x}}{8}K_{ij}K^{ij}\psi^{-7}=0 \quad \text{for } 0\le x\le x_0 , \tag{12}$$

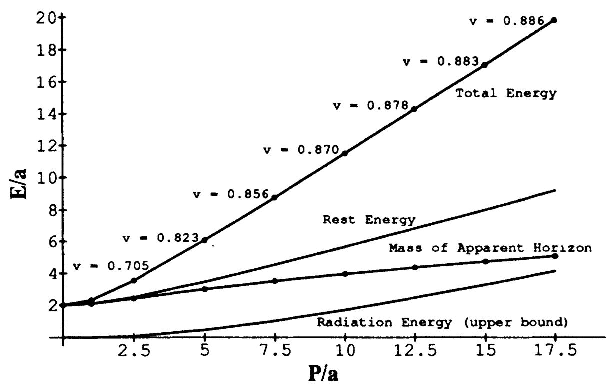

FIG. 1. The energy and velocity for black holes with linear momentum P. a is the radius of the minimal surface.

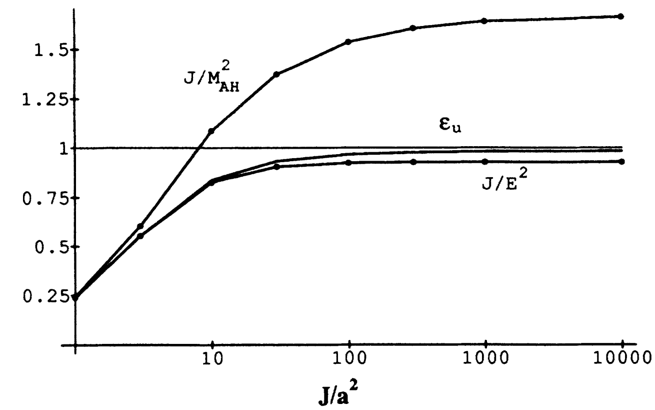

FIG. 2. The angular momentum parameters for black holes with angular momentum J. a is the radius of the minimal surface.

$$\frac{\partial\psi}{\partial x}+\frac{\psi}{2}=0 \quad \text{for } x=0 \;. \tag{13}$$

$$\frac{\partial\psi}{\partial x}+\psi-1=0 \quad \text{for } x=x_0 \;, \tag{14}$$

where x_0 is the location of the outer boundary and we have restricted ourselves to configurations with manifest axial symmetry by taking the linear and angular momentum vectors in the z direction.

These equations were differenced using a conservative second-order differencing scheme and solved using a multigrid algorithm,[7,17] with results comparable to those reported by Choptuik and Unruh,[7] and Rauber[8] to within 2%. Figures 1 and 2 above display results from the numerical solutions for translating and spinning holes which obey the isometry condition (6) with the minus sign. The graph for translating holes which obey (6) with a plus sign conveys no additional information and is not shown. In Fig. 1 we see the calculated values of the total energy and the mass of the apparent horizon. We define the velocity of the holes as $v=P/E$ where E is the total energy, which can be expressed by

$$E=-\frac{1}{2\pi}\int_{r\to\infty}\nabla^i\psi\, d^2S_i \;, \tag{15}$$

for a conformally flat three-metric. We see that the velocity is always less than unity ($c=1$) in accord with the positive-energy theorem. Also plotted in Fig. 1 is the rest energy of the hole defined as $\sqrt{E^2-P^2}$, and an upper limit on the amount of energy available for release as gravitational radiation ($E_{\text{rest}}-M_{\text{AH}}$ where M_{AH} is the mass of the apparent horizon). Figure 2 shows three quantities which are characteristic of rotating holes. Since the initial slices for these rotating holes are (t,ϕ) symmetric but conformally flat, they cannot represent a Kerr black hole.[3] However, from the black-hole uniqueness theorems, it seems that these data will certainly evolve into Kerr geometries after releasing or absorbing the presumably relatively small amount of gravitational radiation coded into the initial data. An extreme Kerr black hole occurs when $\epsilon_k=J/M^2=1$. An upper limit to the final angular momentum parameter associated with our data is given by J/M_{AH}^2 while a lower limit is J/E^2. York and Piran[6] state that a better approximation to the upper limit is given by $\epsilon_u=J/M^2(M_{\text{AH}},J)$ where $M(M_{\text{AH}},J)$ is obtained from the Christoudolou formula[18] for the Kerr metric, but in which M_{AH} has been substituted for the irreducible mass. Tables I–III contain the results of the numerical solutions. These numbers are included for comparison with the numerical results of past authors and for comparison with any future work.

IV. APPARENT HORIZONS IN THE CONFORMAL IMAGING FORMALISM

Hawking and Ellis[9] define an apparent horizon to be the outer boundary of a connected component of a trapped region. A trapped region, in turn, is defined as the collection of all points within all compact orientable spacelike two-surfaces for which the surface-orthogonal outgoing null geodesics have nonpositive expansion. To search for apparent horizons, it will be convenient to look for surfaces with zero expansion. This is a reasonable approach since the hypersurfaces with which we deal are asymptotically flat and do have regions exterior to the horizon with positive expansion. The equations we need can be derived as in Ref. 16. One obtains

$$\bar{\nabla}_i\bar{s}^i-\bar{K}+\bar{K}_{ij}\bar{s}^i\bar{s}^j=0 \;, \tag{16}$$

where $\bar{s}^i$ is the outward pointing spacelike unit normal of the apparent horizon. This is the apparent-horizon equation defined solely in terms of objects defined on the physical hypersurface. We can relate this to the conformally related background three-geometry by defining the unit normal relative to the background metric:

$$\bar{s}^i=\psi^{-2}s^i \;. \tag{17}$$

After some simplification, the apparent-horizon equation becomes

$$\nabla_i s^i+4s^i\nabla_i\ln\psi-\psi^2\bar{K}+\psi^{-4}K_{ij}s^is^j=0 \;. \tag{18}$$

Since the normals to the apparent horizon are surface forming, we can write

$$s_i=\lambda\nabla_i\tau, \quad \lambda=[(\nabla^i\tau)(\nabla_i\tau)]^{-1/2} \;, \tag{19}$$

where τ is a scalar function whose level surface $\tau=\tau_0$ defines the apparent horizon. Using (19) in (18) yields

$$\lambda\nabla^2\tau+(\nabla^i\lambda)(\nabla_i\tau)+4\lambda(\nabla^i\ln\psi)(\nabla_i\tau)-\psi^2\bar{K} + \psi^{-4}\lambda^2 K_{ij}(\nabla^i\tau)(\nabla^j\tau)=0 \ . \quad (20)$$

Because of the inversion symmetry imposed upon the manifold, we expect that any apparent horizon should have an inversion-symmetric counterpart. This can be proved explicitly as follows. As for all fields defined on the manifold, we demand that the unit normal to the apparent horizon should obey the imposed isometry so that

$$\bar{s}^i(x)=\pm(J^{-1})^i_j\bar{s}^j[J(x)] \quad (21)$$

or in terms of the background fields

$$s^i(x)=\pm\left[\frac{a}{r}\right]^2(J^{-1})^i_j s^j[J(x)] \ , \quad (22)$$

where the explicit form of the isometry has been used.

Assume now that $s^i(x)$ is a solution of the apparent-horizon equation, where x belongs to the set of points which satisfy $\tau(x)=\tau_0$. The inversion-symmetric counterpart to this horizon will be labeled $\tilde{s}^i(x)$ where

$$\tilde{s}^i(x)=\pm\left[\frac{a}{r}\right]^2(J^{-1})^i_j s^j[J(x)] \ . \quad (23)$$

Let us use Cartesian coordinates in which the isometry is expressed as

$$J^i(x)=x'^i=\frac{a^2}{r^2}x^i \quad (24)$$

and the Jacobian and inverse Jacobian are explicitly

$$J^i_j(x')=\frac{r'^2}{a^2}(\delta^i_j-2n'^i n'_j) \ ,$$
$$(J^{-1})^i_j(x')=\frac{a^2}{r'^2}(\delta^i_j-2n'^i n'_j) \ , \quad (25)$$

where $n'^i\equiv x'^i/r'$. Using these relations, we find that

$$\nabla_i\tilde{s}^i(x)=\pm\frac{r'^2}{a^2}\left[\nabla'_i s^i(x')-\frac{4}{r'}n'_i s^i(x')\right] \ , \quad (26)$$

$$\tilde{s}^i(x)\nabla_i\ln\psi(x)=\pm\frac{r'^2}{a^2}s^i(x')\left[\nabla'_i\ln\psi(x')+\frac{4}{r'}n'_i\right] \ , \quad (27)$$

and

$$\psi^{-4}(x)K_{ij}(x)\tilde{s}^i(x)\tilde{s}^j(x) =\pm\frac{r'^2}{a^2}\psi^{-4}(x')K_{ij}(x')s^i(x')s^j(x') \ , \quad (28)$$

where we have used the relations[3]

$$\psi(x)=\frac{a}{r}\psi[J(x)] \quad \text{and} \quad K_{ij}(x)=\pm\frac{a^2}{r^2}J^k_i J^l_j K_{kl}[J(x)] \ . \quad (29)$$

Combining (26)–(28) and simplifying, we find that

$$\nabla_i\tilde{s}^i(x)+4\tilde{s}^i(x)\nabla_i\ln\psi(x)+\psi^{-4}(x)K_{ij}(x)\tilde{s}^i(x)\tilde{s}^j(x) =\pm\frac{a^2}{r^2}[\nabla'_i s^i(x')+4s^i(x')\nabla'_i\ln\psi(x')+\psi^{-4}(x')K_{ij}(x')s^i(x')s^j(x')] \ . \quad (30)$$

We know that the right-hand side of (30) is zero when $\tau(x')=\tau_0$. Therefore, $\tilde{s}^i(x)$, as given by (23), is a solution to the apparent-horizon equation where x belongs to the set of points for which $\tau[J(x)]=\tau_0$. Note that it seems necessary to use maximal slicing ($\bar{K}=0$) in order for there to be a manifestly inversion-symmetric horizon. This is also required in order to obtain a manifestly inversion-symmetric solution of the Hamiltonian constraint.

V. METHOD OF FINDING APPARENT HORIZONS

The apparent-horizon equation given in (20) is highly nonlinear and usually must be solved numerically. In this section we set up the equation as a boundary-value problem appropriate for use with the calculated initial data as described above.

The apparent horizons are two-dimensional surfaces, but our initial data sets are axially symmetric so we will only need to solve for a one-dimensional surface. Using the coordinate system described by (11) we choose τ to be

$$\tau(x,\theta)=x-h(\theta) \quad (31)$$

and choose the level surface generated by $\tau=0$ to be the apparent horizon. This choice defines the radius of the apparent horizon parametrically as $x=h(\theta)$. Some straightforward calculations give

$$h_{,\theta\theta}+[\cot(\theta)+4\psi^{-1}\psi_{,\theta}]h_{,\theta}(1+h^2_{,\theta})+(-2-4\psi^{-1}\psi_{,x})(1+h^2_{,\theta}) -e^{-x}\sqrt{1+h^2_{,\theta}}\,\psi^{-4}\left[\frac{K_{xx}}{a}+\frac{K_{\theta\theta}}{a}h^2_{,\theta}-2\frac{K_{x\theta}}{a}h_{,\theta}\right]=0, \quad \theta\neq 0,\pi \quad (32a)$$

and

$$(2+h_{,\theta}^2)h_{,\theta\theta}+4\psi^{-1}\psi_{,\theta}h_{,\theta}(1+h_{,\theta}^2)+(-2-4\psi^{-1}\psi_{,x})(1+h_{,\theta}^2)$$
$$-e^{-x}\sqrt{1+h_{,\theta}^2}\,\psi^{-4}\left[\frac{K_{xx}}{a}+\frac{K_{\theta\theta}}{a}h_{,\theta}^2-2\frac{K_{x\theta}}{a}h_{,\theta}\right]=0,\quad \theta=0,\pi \qquad (32b)$$

where all functions of x are evaluated at $x=h(\theta)$. The relevant components of the extrinsic curvatures for spin angular momentum defined in (9) are identically zero. The relevant components for linear momentum as given in (8) are as follows:

$$\frac{K_{xx}^{\pm}}{a}=6\left[\frac{P}{a}\right]e^{-x}\begin{Bmatrix}\cosh(x)\\ \sinh(x)\end{Bmatrix}\cos(\theta)\ , \qquad (33)$$

$$\frac{K_{\theta\theta}^{\pm}}{a}=-3\left[\frac{P}{a}\right]e^{-x}\begin{Bmatrix}\cosh(x)\\ \sinh(x)\end{Bmatrix}\cos(\theta)\ , \qquad (34)$$

$$\frac{K_{x\theta}^{\pm}}{a}=-3\left[\frac{P}{a}\right]e^{-x}\begin{Bmatrix}\sinh(x)\\ \cosh(x)\end{Bmatrix}\sin(\theta)\ . \qquad (35)$$

The domain over which (32) must be solved is $0\le\theta\le\pi$. In order to solve (32) as a boundary-value problem, we must specify boundary conditions at $\theta=0,\pi$. Since the solution must be axially symmetric, we demand that $\partial h/\partial\theta=0$ at the boundaries.

At this point, we have a well-posed though highly nonlinear problem. There is quite a bit of information which can be gleaned about the solutions of (32) for each of the specific forms of the extrinsic curvature before passing to numerical methods. We know that for the time-symmetric problem ($K_{ij}=0$), the apparent horizon is coincident with the minimal surface; therefore, the vanishing of the first three terms of (32) alone is a minimal-surface equation. Since the contributing components of the extrinsic curvature for holes with only spin angular momentum are zero on the minimal surface, we know that the apparent horizon for a spinning conformally imaged hole must be coincident with the minimal surface.

If we now consider the K_{ij}^- solutions, we notice that on the minimal surface $K_{xx}^-=K_{\theta\theta}^-=0$. If we guess that $h(\theta)=0$ is a solution, then the contribution of $K_{x\theta}^-$ is nullified since it is multiplied by $h_{,\theta}$ which is zero. $h(\theta)=0$ is of course the minimal surface and will certainly cause the first three terms of (32) to vanish. Therefore, it is a solution of the full apparent-horizon equation. This does not preclude the existence of other apparent horizons, but their existence must be examined numerically. York and Piran[6] stated that $K_{ij}s^is^j\neq0$ at the minimal surface and that the minimal surface and apparent horizon cannot coincide in the case we are currently discussing. While this is true for an arbitrary vector s^i, we have shown that if s^i is a unit normal to the minimal surface, then $K_{ij}s^is^j=0$. The apparent horizon found numerically in Ref. 6 to be slightly outside the minimal surface, therefore, does not exist.

Finally, if we consider the K_{ij}^+ solutions and ask whether $h(\theta)=0$ is a solution, we find that this can be so only if $K_{xx}^+=0$ for all θ. But this requires $P=0$, which is simply the Schwarzschild solution. Thus, the minimal surface and an apparent horizon cannot coincide if $P\neq0$ in this case.

Before solving this problem numerically, we can anticipate the form of the apparent horizon for the K_{ij}^+ solutions by looking at the case of slowly moving Schwarzschild black holes. Bowen and York[3] examined the effect of Lorentz boosting a Schwarzschild black hole to first order in the boost velocity. After demanding that the boosted slice be maximal, the metric is found, as expected, to be unchanged through first order in the boost velocity. Thus

$$\bar{g}_{ij}=\left[1+\frac{a}{r}\right]^4 g_{ij}=\psi^4 g_{ij}\ , \qquad (36)$$

where g_{ij} is, as before, the flat background metric. The boosted form of the extrinsic curvature is, to first order, just

$$\bar{K}_{ij}=\psi^{-2}K_{ij}^{\pm}\ , \qquad (37)$$

where $P_i=MV_i=2aV_i$ and V_i is the velocity of the boost. The two forms which the boosted extrinsic curvature take correspond to two possible inversion symmetric choices for the lapse function.

We can now examine the apparent horizons of these slowly moving black holes. In addition to having analytic solutions for the extrinsic curvature (33)–(35), we also have, in the present case, an analytic form for the conformal factor which can be inserted in the apparent-horizon equation (32). Using

$$\psi=1+e^{-x}\ , \qquad (38)$$

we find that the apparent-horizon equation becomes

$$h_{,\theta\theta}+\cot(\theta)h_{,\theta}(1+h_{,\theta}^2)+\left[-2+\frac{2e^{-h/2}}{\cosh(h/2)}\right](1+h_{,\theta}^2)$$
$$-\frac{e^h}{16\cosh^4(h/2)}(1+h_{,\theta}^2)^{1/2}\left[\frac{K_{xx}}{a}+\frac{K_{\theta\theta}}{a}h_{,\theta}^2-2\frac{K_{x\theta}}{a}h_{,\theta}\right]=0\ . \qquad (39)$$

If we choose the K_{ij}^- solutions, we find as above that $h(\theta)=0$ is a solution for slowly moving holes and the apparent horizon and minimal surface coincide. Similarly, if we choose the K_{ij}^+ solutions, we again find that the apparent horizon and minimal surface cannot coincide. To proceed, let us guess a solution and take

$$h(\theta)=H\cos(\theta) . \quad (40)$$

For a slowly moving hole, we expect that the coefficient H will be small so that the apparent horizon will not deviate far from the minimal surface. Inserting (40) and (33)–(35) into (39) and expanding the result through first order in H, we find that (40) is indeed a solution of the apparent-horizon equation if

$$H=-\frac{3}{8}\frac{P}{a} . \quad (41)$$

Thus, the resulting apparent-horizon function $h(\theta)$ is first order in the boost velocity which is consistent with all of the assumptions of the derivation. The consequences of this form for the configuration of the apparent horizon and minimal surface will be discussed below. For the present, we note that because P/a is small, the radius of the apparent horizon can be expressed as $r\simeq a[1+H\cos(\theta)]$. Thus, the apparent horizon can be regarded as a *translation* ($P_l=\cos(\theta);l=1$) of the minimal surface.

VI. SOLVING FOR APPARENT HORIZONS NUMERICALLY

In order to find the apparent horizons for conformally imaged black holes we must solve (32) numerically. Equations (32a) and (32b) were differenced using second-order central difference operators resulting in a set of nonlinear algebraic equations. This set of equations was solved using Newton's method for nonlinear systems of equations.[19] This method employs a trial solution to generate a linear equation for a correction to the trial solution. The resulting linearized equation is tridiagonal in our case and was solved directly. The process of linearizing around a trial solution and generating a correction is iterated until the magnitude of the correction and the magnitude of the residuals of the apparent-horizon equation are sufficiently small.

There is one difficult point in evaluating the differenced apparent-horizon equation. The equation depends upon ψ and its derivatives which are known only numerically on a discrete grid. We can guarantee that we will evaluate ψ and its derivatives only on lines of constant θ which match the gridding used for calculating ψ by carefully choosing the discretization of the apparent-horizon equation. However, on any given line of constant θ, the radial position at which ψ and its derivatives must be evaluated depends on the current estimate of the position of the apparent horizon. This certainly cannot be constrained to be at a radius coinciding with any line of constant radius on the ψ grid.

To cope with this problem, we have used cubic splines to interpolate function values at any radius along each grid line of constant θ. Because derivatives of ψ are also required, we have factored out the gross behavior of the solution so that the resulting numerical data only reflects a small, slowly varying function which we call $C(x,\theta)$ (Ref. 20). We take

$$\psi(x,\theta)=f(x)C(x,\theta) \quad \text{where } f(x)\equiv 1+\frac{1}{2}\frac{E}{a}e^{-x} \quad (42)$$

and E/a is the scaled total energy of the solution. Radial derivatives are evaluated by taking derivatives of the cubic spline interpolation scheme and angular derivatives are evaluated numerically to second order.

While the function ψ is only determined numerically in the range $0\le x\le x_0$ and $0\le\theta\le\pi/2$, we will need to evaluate the function over the range $-\infty<x<\infty$ and $0\le\theta\le\pi$. This can be handled easily since we know $\psi(\pi/2+\theta)=\psi(\pi/2-\theta)$ and from the isometry condition, $\psi(x<0)=e^{|x|}\psi(|x|)$. Finally, if ψ is needed for $|x|>x_0$ (and this is not likely to be necessary), it can be approximated by $\psi(x>0)\approx f(x)$ which is the approximation used to derive the outer boundary condition.

Some of the results of the numerical calculations are listed in Tables I–III below. Tables I and II list the results for black holes with spin and linear momentum, respectively, and which satisfy the isometry condition (6) with a minus sign. These two tables list, for each value of the angular or linear momentum, the total energy of the slice and the mass of the apparent horizon (M_{AH}/a), which is the same as that of the minimal surface (M_{MS}/a). Here, the mass is defined similarly to irreducible mass by

$$M=\sqrt{A/16\pi} , \quad (43)$$

where A is the area of the surface in question. As expect-

TABLE I. Scaled energy and apparent-horizon mass for black holes with angular momentum J.

J/a^2	Energy/a	M_{AH}/a
1	2.048	2.033
3	2.329	2.227
10	3.477	3.034
30	5.759	4.673
100	10.41	8.071
300	17.99	13.67
1000	32.83	24.69
10 000	103.8	77.56

TABLE II. Scaled energy and apparent-horizon mass for black holes with linear momentum P and with extrinsic curvature K_{ij}^-.

P/a	Energy/a	M_{AH}/a
0	2.000	2.000
1	2.330	2.100
2.5	3.545	2.430
5	6.078	3.001
7.5	8.760	2.502
10	11.49	3.946
12.5	14.24	4.348
15	17.00	4.716
17.5	19.76	5.058

TABLE III. Scaled energy, minimal-surface mass and apparent-horizon mass for black holes with linear momentum P and with extrinsic curvature K_{ij}^{+}. Also tabulated are the apparent-horizon coefficient H and its standard deviation σ as given by a least-squares fit of the apparent-horizon data to the proposed apparent-horizon function.

P/a	Energy/a	M_{MS}/a	M_{AH}/a	$H(P/a)$	σ
1	2.347	2.113	2.119	−0.112 291	0.000 012
2.5	3.589	2.470	2.496	−0.206 398	0.000 087
5	6.133	3.069	3.121	−0.269 071	0.000 21
7.5	8.815	3.589	3.662	−0.295 948	0.000 29
10	11.54	4.049	4.138	−0.310 731	0.000 34
12.5	14.29	4.463	4.567	−0.320 063	0.000 39
15	17.04	4.843	4.959	−0.326 486	0.000 41
17.5	19.81	5.195	5.324	−0.331 175	0.000 43
50	55.93	8.550	8.784	−0.350 327	0.000 53
100	111.6	12.00	12.34	−0.355 751	0.000 56
1000	1117	37.71	38.80	−0.360 762	0.000 58

ed, an apparent horizon was found in each case which coincided with the minimal surface to well within truncation error. No other solutions were found.

Table III lists the results for black holes with linear momentum satisfying the isometry condition (6) with a plus sign. Table III lists both (M_{MS}/a) and (M_{AH}/a) as well as two additional quantities described below. We see immediately, however, that the masses (or areas) of the apparent horizon and of the minimal surface are not the same. Figure 3 shows the shape of the apparent-horizon function $h(\theta)$ for the case of $P/a=10$.

The general sinusoidal shape of the solution is generic to all of the solutions and, in fact, we find to within truncation error that the results can be expressed in the form

$$h(\theta)=H(P/a)\cos(\theta) \quad (44)$$

for all solutions, thereby demonstrating a close resemblance to (40) and (41). In Table III, the column headed by $H(P/a)$ lists the value of the coefficient resulting from a linear least-squares fit of (44) to the data. The column headed by σ lists the standard deviation of the fit. Figure 4 shows a plot of the coefficient $H(P/a)$ showing all calculated points. We have attempted to find an analytic representation for the function $H(P/a)$ but have been unsuccessful.

Given an explicit form of the apparent-horizon function $h(\theta)$, we can construct the outward-pointing unit normals to the surface. From (31) and (44) we find that the function

$$\tau(x,\theta)=x-H(P/a)\cos(\theta)=0 \quad (45)$$

defines the surface of the apparent horizon and thus, from (19),

$$s^{i}(\theta,P/a)=\frac{1}{ae^{H(P/a)\cos(\theta)}\sqrt{1+H^2(P/a)\sin^2(\theta)}}\times[1,H(P/a)\sin(\theta),0]\ . \quad (46)$$

We see that the surface normals point in the general direction of increasing radial coordinate. Thus, this surface is an apparent horizon for observers on the top sheet.

An interesting feature of the apparent horizon is that it is *inside* the minimal surface for $0\le\theta<\pi/2$ and outside for $\pi/2<\theta\le\pi$. The momentum vector for the black hole, as measured by observers at infinity, is in the $\theta=0$ direction so the apparent horizon is inside the minimal surface on the *leading* face of the black hole.

We showed above that there must be an inversion symmetric counterpart to this apparent horizon. We find from inversion symmetry that it is defined by

$$\tau(x,\theta)=-x-H(P/a)\cos(\theta)=0 \quad (47)$$

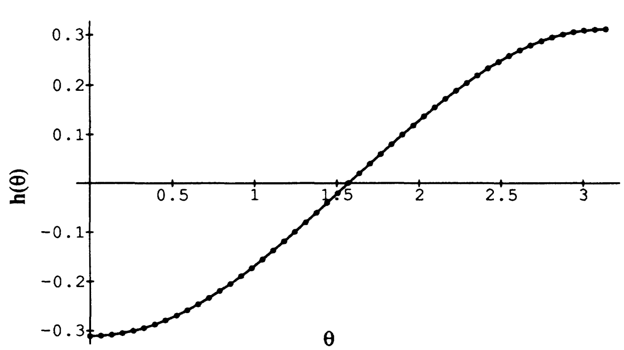

FIG. 3. The apparent-horizon function for a hole with linear momentum $P/a=10$.

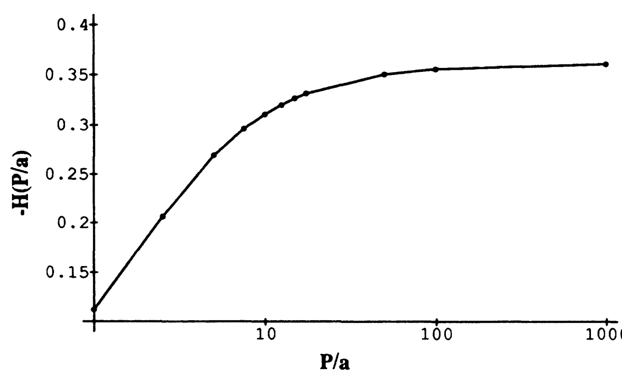

FIG. 4. The apparent-horizon coefficient H as a function of P/a.

and from (23) written in terms of our coordinate system we find that

$$\tilde{s}^i(\theta,P/a)=\frac{1}{ae^{H(P/a)\cos(\theta)}\sqrt{1+H^2(P/a)\sin^2(\theta)}}\times[-1,H(P/a)\sin(\theta),0]\ . \qquad (48)$$

In this case, the surface normals point in the general direction of decreasing radial coordinate. Thus, the inversion symmetric apparent horizon is a horizon for observers on the bottom sheet.

VII. DISCUSSION

From past experience, we would have expected that the apparent horizon for the top sheet would have been positioned exterior to the minimal surface so as to be completely in the top sheet. Its inversion symmetric counterpart, the apparent horizon for the bottom sheet, would then have been positioned interior to the minimal surface so as to be completely in the bottom sheet. With this structure, the initial hypersurface would consist of three distinct regions: an unbounded region for each of the two sheets and a trapped region between the two apparent horizons.

Our calculations have shown, however, that the two isometric apparent horizons given in (45) and (47) do not follow this expected behavior. Both apparent horizons cross the minimal surface and each other. In Fig. 5 we illustrate the general relationships between the various surfaces as they appear on the conformal background space. For this diagram, we have returned to a standard radial coordinate $r=ae^x$ so that the minimal surface is at $r=a$, the upper sheet is $r>a$, and the bottom sheet is $r<a$. Note that asymptotic infinity on the bottom sheet has now been conformally transformed to the origin in this coordinate system.

For $\pi/2<\theta\le\pi$, the top-sheet apparent horizon is in the top sheet and the bottom-sheet apparent horizon is in the bottom sheet. They intersect each other and the minimal surface at $\theta=\pi$. The region between the two apparent horizons, for this range of θ, is a trapped region behaving as we would previously have expected. This region is shaded darkest in Fig. 5.

For $0\le\theta<\pi/2$, the top-sheet apparent horizon is in the bottom sheet and the bottom-sheet apparent horizon is in the top sheet. We would normally expect these "conjugate" apparent horizons to be inaccessible to observers who are not trapped. Since they are accessible, they create an excluded region between the two apparent horizons. This region is shaded lightly in Fig. 5. In a certain sense, this region acts like a white hole. That is, for this range of θ, the bottom- (top-) sheet apparent horizon is acting as a past apparent horizon for the top (bottom) sheet.

Figure 6 represents the same scenario in the physical space using an embedding diagram. This diagram shows more clearly the isometric bottom sheet. An observer at infinity on the top sheet sees the hole moving in the $\theta=0$ direction with momentum P/a and an observer at infinity on the bottom sheet also sees the hole moving in the $\theta=0$ direction with momentum P/a. In contrast with this, if

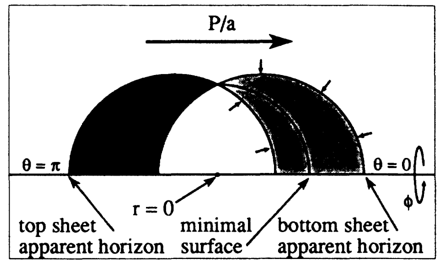

FIG. 5. Relation of the apparent horizons to the minimal surface on the conformal background geometry.

Fig. 6 represents a hole with momentum P/a generated from K^-_{ij}, then the apparent horizons for both sheets would be coincident with the minimal surface, and an observer on the bottom sheet would measure the momentum to be directed towards $\theta=\pi$.

It has long been known that solutions generated from K^-_{ij} resemble what one would expect for the behavior of a translating hole formed from the collapse of matter.[2] To the best of our knowledge, however, solutions generated from K^+_{ij} have never been successfully related to matter solutions. The reason for this seems clear given the structure of the apparent horizons for the K^+_{ij} solutions because we know that past horizons are only seen in eternal black-hole solutions (or in "white" hole solutions) and are not seen for black holes formed from gravitational collapse.

The behavior we have described for the apparent horizon generated by K^+_{ij} can be understood qualitatively from the discussion of boosted maximal slices of the Schwarzschild-Kruskal space-time given above. There, the evolution of data corresponding to K^+_{ij} and to K^-_{ij}, and their maximal analytic extensions, must result in the same global space-time. That cannot literally be the case for our data, however, because as reference to Tables II and III shows, the total energies are different for K^+_{ij} and K^-_{ij} even when their respective momenta are precisely equal. Nevertheless, we expect in a time evolution that

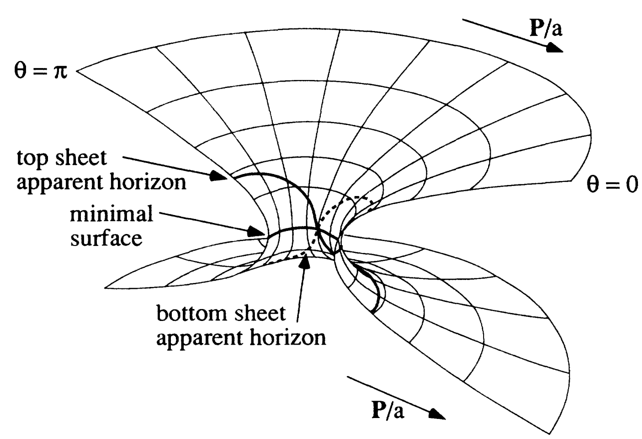

FIG. 6. Embedding diagram illustrating the position of the apparent horizons.

the two global space-times would "settle down," each to a Schwarzschild-Kruskal space-time described by boosted maximal slices. That is, each of our data sets already closely resembles a boosted slice through the Schwarzschild-Kruskal space-time except that each has some extra structure ("hair"). (For example, our three-metrics are conformally flat, but this does not hold for a boosted maximal slice in the Schwarzschild-Kruskal space-time.) We expect the extra structure to "radiate away" or be "swallowed up" as time elapses. Furthermore, it has been suggested that horizon structure similar to that which we have found could be seen on an appropriately chosen slice of the Schwarzschild-Kruskal space-time.[21] In any case, a fuller understanding will require an evolution of the data, which we hope to accomplish soon.

It has been proposed by Unruh and Thornburg[22] that using the minimal-surface inner boundary condition (10) is inefficient since "this boundary condition results in the (modeled) interior of each black hole being in some sense a "mirror image" of the (modeled) rest of the space, which we consider somewhat unnatural." They propose and use an inner boundary condition based on the apparent-horizon equation (18). Using the conformally imaged solutions of the momentum constraint, they solve the Hamiltonian constraint using a boundary condition which forces the inner boundary to be an apparent horizon. This horizon will, by construction, be a future apparent horizon. We can see, of course, that without knowing the solution within this horizon there is no way of finding the second apparent horizon. One would normally assume that this second horizon is not part of the geometry of the top sheet, making it irrelevant. However, we clearly see from our example that this is not necessarily the case.

The topology of the initial hypersurface for vacuum black-hole initial-data sets is completely undetermined by Einstein's equations. The space-time resulting from the evolution of any such initial-data set will necessarily reflect the choice of topology for this initial hypersurface. While an observer exterior to an apparent horizon will never be able to receive information from sources within the apparent horizon, this is completely unrelated to the fact that the geometry exterior to the apparent horizon is affected by the geometry interior to it in the sense that the interior geometry is part of a global construction. That is, the conformal imaging technique enables the construction of a *complete* manifold as an initial data slice. This should make more of the global structure of the evolving space-time accessible in the numerical evolution. Experience with the known, exact black-hole space-times has fully demonstrated the value of probing global space-time geometry.

ACKNOWLEDGMENTS

We would like to thank Tsvi Piran, Steven Detweiler, Kent Blackburn, and especially Bernard Whiting for valuable discussions. We thank the National Science Foundation for partial support through grants at the University of North Carolina.

[1]J. W. York, Jr., in *Sources of Gravitational Radiation,* edited by L. L. Smarr (Cambridge University Press, London, 1979).

[2]J. Bowen, Gen. Relativ. Gravit. **11**, 227 (1979).

[3]J. Bowen and J. W. York, Jr., Phys. Rev. D **21**, 2047 (1980).

[4]J. Bowen, Gen. Relativ. Gravit. **14**, 1183 (1982).

[5]A. D. Kulkarni, L. C. Shepley, and J. W. York, Jr., Phys. Lett. **96A**, 228 (1983).

[6]J. W. York, Jr., and T. Piran, in *Spacetime and Geometry: The Alfred Schild Lectures,* edited by R. Matzner and L. Shepley (University of Texas Press, Austin, 1982), pp. 147–176.

[7]M. Choptuik and W. G. Unruh, Gen. Relativ. Gravit. **18**, 813 (1986).

[8]J. D. Rauber, Ph.D. dissertation (University of North Carolina, 1985).

[9]S. W. Hawking, and G. F. R. Ellis, *The Large Scale Structure of Space-Time* (Cambridge University Press, London, 1973).

[10]A. Čadež, Ann. Phys. (N.Y.), **83**, 449 (1974).

[11]N. T. Bishop, Gen. Relativ. Gravit. **14**, 717 (1982).

[12]N. T. Bishop, Gen. Relativ. Gravit. **16**, 589 (1984).

[13]T. Nakamura, Y. Kojima, and K. Oohara, Phys. Lett. **106A**, 235 (1984).

[14]K. Oohara, T. Nakamura, and Y. Kojima, Phys. Lett. **107A**, 452 (1985).

[15]C. W. Misner, Ann. Phys. (N.Y.) **24**, 102 (1963).

[16]J. W. York, Jr., in *Frontiers in Numerical Relativity,* edited by C. R. Evans, L. S. Finn, and D. W. Hobill (Cambridge University Press, London, 1989).

[17]G. B. Cook, in *Frontiers in Numerical Relativity* (Ref. 16).

[18]D. Christodoulou, Phys. Rev. Lett. **25**, 1596 (1970).

[19]W. H. Press, B. P. Flannery, S. A. Teukolsky, and W. T. Vetterling, *Numerical Recipes in C* (Cambridge University Press, London, 1988).

[20]T. Piran (private communication).

[21]S. Detweiler (private communication).

[22]J. Thornburg, Class. Quantum Grav. **4**, 1119 (1987).

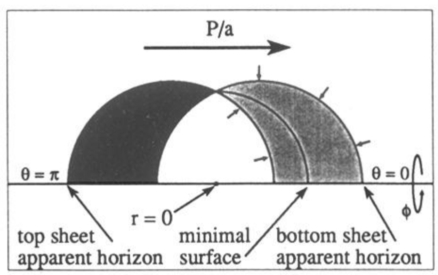

FIG. 5. Relation of the apparent horizons to the minimal surface on the conformal background geometry.